Title
Mechanistic Insights into the Origins of Selectivity in a Cu-Catalyzed C—H Amidation Reaction

Journal
Journal of the American Chemical Society, 146(9)

ISSN
0002-7863

Authors
Sterling, Alistair J
Ciccia, Nicodemo R
Guo, Yifan
et al.

Publication Date
2024-03-06

DOI
10.1021/jacs.3c13822

Mechanistic insights into the origins of selectivity in a Cu-catalyzed C–H amidation reaction

Alistair J. Sterling,*[†§‡] Nicodemo R. Ciccia,[†§‡] Yifan Guo,[†] John F. Hartwig,*[†§] Martin Head-Gordon*[†§]

[†]Department of Chemistry, University of California, Berkeley, California, 94720, United States
[§]Chemical Sciences Division, Lawrence Berkeley National Laboratory, Berkeley, California, 94720, United States

KEYWORDS Catalysis, C–H functionalization, computation, energy decomposition analysis

ABSTRACT: The catalytic transformation of C–H to C–N bonds offers rapid access to fine chemicals and high-performance materials, but achieving high selectivity from undirected aminations of unactivated C(sp^3)–H bonds remains an outstanding challenge. We report the origins of reactivity and selectivity of a Cu-catalyzed C–H amidation of simple alkanes. Using a combination of experimental and computational mechanistic studies and energy decomposition techniques, we uncover a switch in mechanism from inner-sphere to outer-sphere coupling between alkyl radicals and the active Cu(II) catalyst with increasing substitution of the alkyl radical. The combination of computational predictions and detailed experimental validation shows that simultaneous minimization of both Cu–C covalency and alkyl radical size increases the rate of reductive elimination, and that both strongly electron-donating and electron-withdrawing substituents on the catalyst accelerate the selectivity-determining C–N bond formation process as a result of a change in mechanism. These findings offer design principles for the development of improved catalyst scaffolds for radical C–H functionalization reactions.

Introduction

Selective reactions of unactivated C(sp^3)–H bonds enable rapid diversification of a wide range of compounds.[1–6] In particular, methods for the amination of alkyl C–H bonds have the potential to provide direct access to *N*-alkyl amine derivatives in complex molecules or high-performance materials without the need for preinstalled reactive functionality.[1,2] Significant progress has been made towards the development of catalytic, intermolecular C–H aminations that involve metallacyclic, metal-nitrenoid, or free radical intermediates (Figure 1a), but most methods require activated C–H bonds or rely on directing groups to achieve the desired selectivity.[7–9] Undirected aminations of tertiary and benzylic C(sp^3)–H bonds have been accomplished by metal-nitrenoid intermediates,[10–13] but reactions at secondary C–H bonds[14] and analogous transformations involving free radical intermediates with high yields and regioselectivity remain challenging to achieve.

Recently, our group and others have reported copper-catalyzed aminations of alkyl C–H bonds with peroxides as oxidants (Figure 1b)[15–25] under conditions similar to the Kharasch-Sosnovsky oxidation of allylic C–H bonds.[26] Such amination reactions create *N*-alkyl amides, carbamates, imides, sulfonamides, amines, sulfoximines, and ureas. However, these transformations are largely limited to the amination of cyclic or benzylic substrates. Reactions of sterically hindered branched alkanes often occurred in low yields, and the selectivity of such reactions followed the general trend of 2°>1°>3° C–H bonds.

Based on a series of mechanistic experiments, we previously proposed that the copper-catalyzed amidation involves alkyl radical intermediates.[15] These experiments provided evidence that the alkyl radical intermediate was generated by hydrogen-atom transfer (HAT) from *tert*-butoxy radical and that monomeric (phenanthroline)Cu(II) bisimidate complexes react with the radical to form the C–N bond (Figure 1c). Given the known selectivity of HAT by *tert*-butoxy radical,[27] it is likely that tertiary, secondary, and primary alkyl radicals are all formed; however, no products from amidation at tertiary or hindered secondary C–H bonds were observed in

reactions of branched alkanes. These results suggest that the hindered radicals do not react with the active copper complex to form product. This disparity between the selectivity of HAT versus the selectivity of productive trapping likely leads to the low yields and poor selectivity for reactions of branched alkanes.

Here, we evaluate by DFT computational methods three mechanistic pathways that could lead to this transformation and identify competing processes that lead to the formation of side products. We use a combination of experimental and computational mechanistic studies, alongside linear energy decomposition relationships, to determine factors that affect the selectivity of the amidation of the C–H bonds of branched alkanes (Figure 1d). Investigations of Cu–C interactions in the putative Cu(III) complex and of a competitive outer-sphere pathway reveal a switch in mechanism that results from the interplay of covalency of the Cu–C bond and steric properties of the alkyl radical that, together, determine the rate of reductive elimination. Experimental investigations of the role of ligand electronic properties on product selectivity corroborate these computational mechanistic conclusions. Ultimately, these results reveal factors for catalyst design that will enable the development of more efficient aminations of branched alkanes.

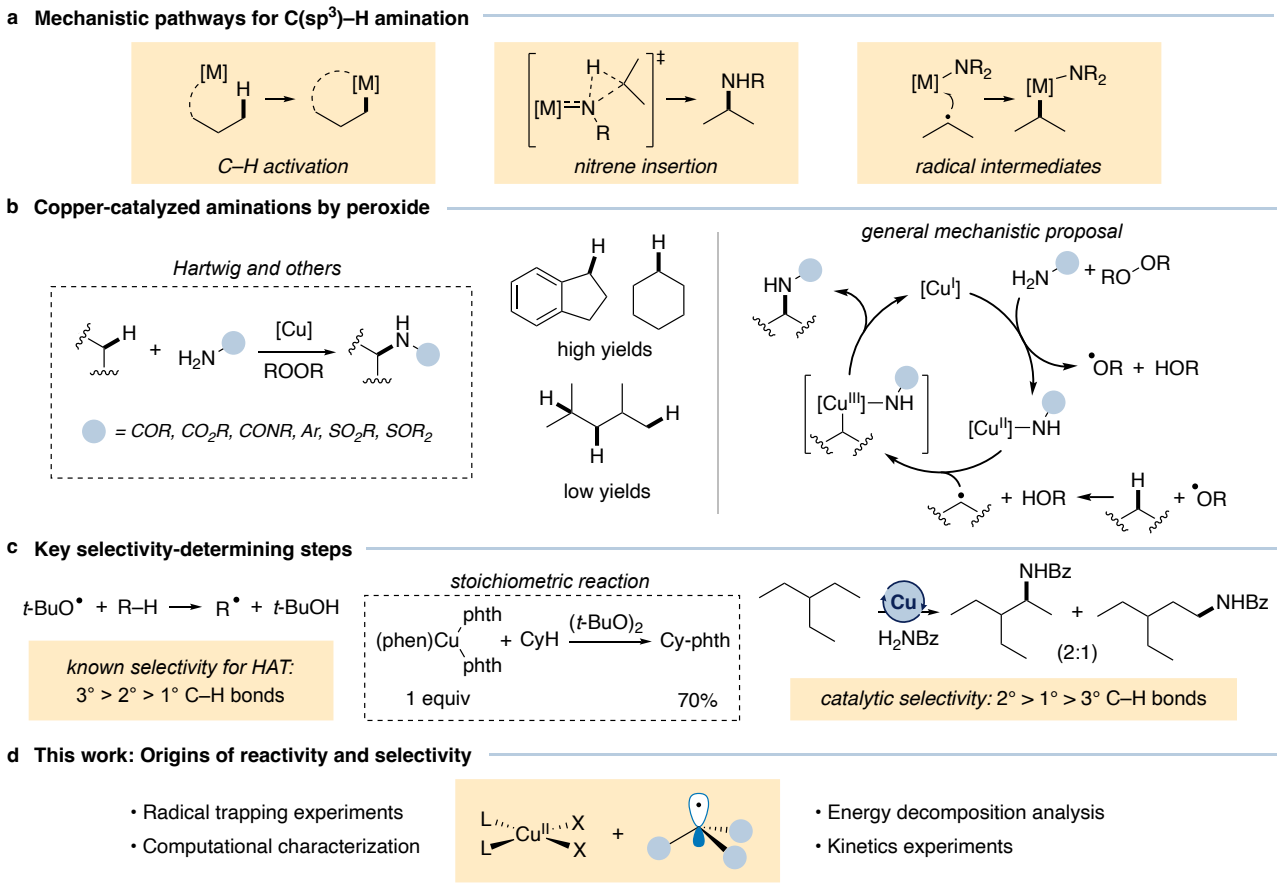

Figure 1. a. Recent developments in the amination of C(sp^3)–H bonds. **b.** Copper-catalyzed aminations of C(sp^3)–H by Hartwig and others.[15–24] **c.** Identification of key processes that determine selectivity.[15] **d**. Uncovering design principles for C–H functionalization through a combined computational / experimental study.

Results and Discussion

Selectivity of alkyl radical trapping. We began our investigations by probing H-atom transfer (HAT) as the possible selectivity-determining step. It was previously determined that irreversible, turnover-limiting HAT occurs between the *tert*-butoxy radical and the alkane (Figure 2a).[15] If this step were also selectivity determining, the ratio of amidation products would match the ratio of alkyl radicals generated by the HAT step. To quantify this relationship, we performed trapping experiments in which superstoichiometric quantities of CBr_4 were used to intercept the alkyl radicals generated by HAT. The selectivity of the bromination products from reactions under conditions of the amidation process, but with the added CBr_4, was compared to that of the amidation reaction in the absence of CBr_4. As illustrated in Figure 2a, the ratio of products from reaction of 2,4-dimethylpentane in the presence of CBr_4 followed the general trend of 3°>2°>1°, whereas the product from the amidation of this alkane in the absence of CBr_4 was solely the 1° *N*-alkyl benzamide product.

These results illustrate that HAT determines the selectivity of radical generation, but the relative rates of radical trapping controls the ratio of final products. In particular, tertiary alkyl radicals and sterically-hindered secondary alkyl radicals are trapped less efficiently by a putative (phen)Cu(NHBz)$_2$ than by CBr_4. We hypothesize that radical decomposition, for instance through $\boldsymbol{\beta}$-scission (Figure 2b), outcompetes the productive Cu-mediated process, thereby resulting in the low yields and product distributions containing only primary or non-hindered secondary alkyl amide products. Indeed, analysis of the headspace of the reaction of 2,4-dimethylpentane indicates that propene and isobutene form, revealing that β-scission of the alkyl radicals do occur in competition with productive amidation (see Figure S4). The formation of methane was also observed. Methyl radicals can be generated in the reaction by β-scission of the 2,4-dimethylpentyl radical or by $\boldsymbol{\beta}$-scission of *tert*-butoxy radicals (Figure 2b).[28–30]

Active copper species. To investigate the selectivity of the combination of these alkyl radicals with the copper catalyst, we first calculated the structure of a putative active catalyst based on previously reported structures of related complexes determined by single-crystal x-ray diffraction. τ_4 values of 0 and 1 indicate perfect D_{4h} and T_d structures of related complexes, respectively.[15] The active Cu(II) bisamidate complex adopts a distorted square planar geometry (Figure 3a) characterized by computed τ_4 values of 0.25 and 0.15 for benzoyl and phthalimide ligands, respectively (Figure 3a and SI Table S3).[31] The Cu d^9 electron count results in a first-order Jahn-Teller distortion to relieve orbital degeneracy in the T_d geometry, with further preference for the more planar, D_{4h}-like geometry in part from π back-bonding of the phen ligand with the metal d orbitals.[32–35] Unpaired spin density is localized primarily in a Cu $d_{x^2-y^2}$ orbital and the corresponding $\boldsymbol{\sigma}^*$ orbitals of the four Cu–N bonds (Figure 3a). Because Cu(I)-mediated reduction of di-*tert*-butyl peroxide produces an equivalent of *tert*-butanol, heteroleptic Cu(II) species (*e.g.*, (phen)Cu(O^{t}Bu)(NHBz)) may be present in the reaction, along with the bisamidate (phen)Cu(NHBz)$_2$. However, the calculated equilibrium between (phen)Cu(NHBz)$_2$ and (phen)Cu(O^{t}Bu)(NHBz) favors the bisamidate complex (ΔG = +4.5 kcal mol^{-1}, see SI Figure S5), supporting the proposal that (phen)Cu(NHBz)$_2$ is an intermediate in the C–H functionalization reaction.

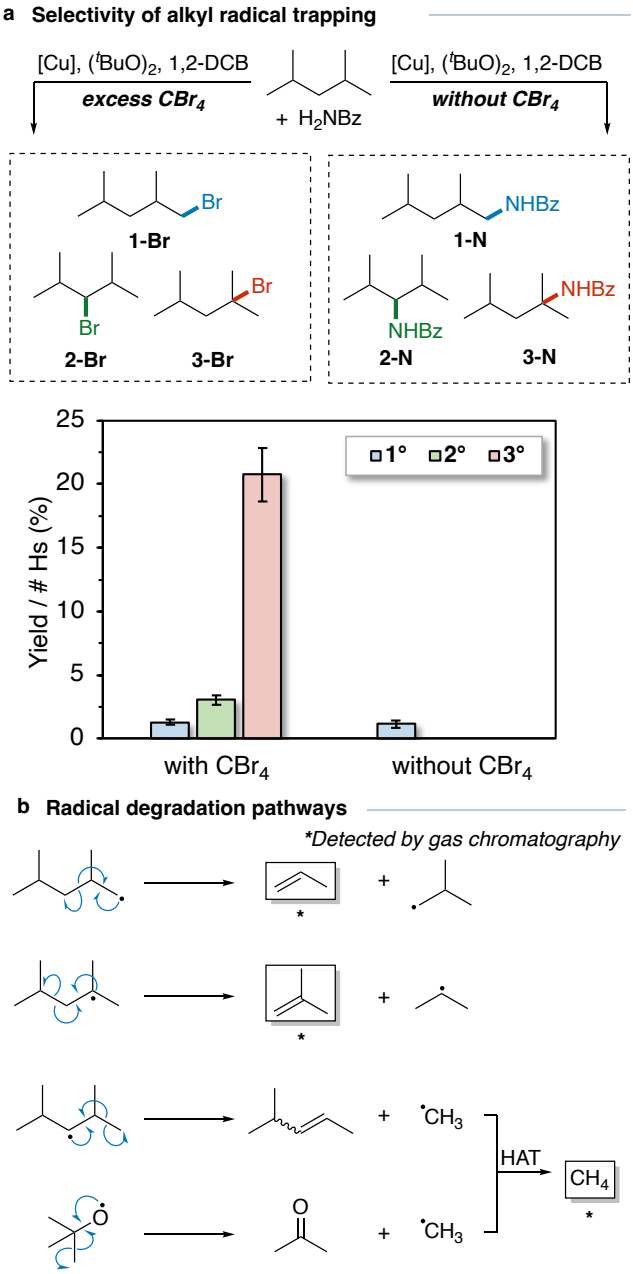

Figure 2. a. Selectivity of alkyl radical trapping indicates that radical formation is more efficient for more substituted radicals, but the substituted radicals are trapped inefficiently by (phen)Cu(NHBz)$_2$. Product yields are reported as the average yield from three experiments, and are normalized for the number of C–H bonds of each type. Error bars denote ±1 σ of the mean. Conditions: 0.3 mmol benzamide, 9 μmol CuI, 9 μmol phen, 12 mmol 2,4-dimethylpentane, 0 or 1.5 mmol carbon tetrabromide, 0.6 mmol (^{t}BuO)$_2$, 1,2-DCB, 120 °C, 24 h. Yields were determined by quantitative ^{1}H NMR spectroscopy and GC-FID. **b.** Proposed mechanistic pathways for the formation of propene, isobutylene, and methane in the amidation of 2,4-dimethylpentane.

Mechanistic trichotomy. The productive trapping of an alkyl radical by this Cu bisamidate could occur by three distinct mechanistic pathways (Figure 3b).[36,37] The first involves single-electron transfer (SET) in which an alkyl cation, formed by one-electron oxidation by the Cu(II) catalyst, is attacked by an amide nucleophile. Such a radical-polar crossover was suggested to be part of the mechanism for the Cu-catalyzed azidation of benzylic C–H bonds.[37] The second mechanistic possibility, proposed to occur during the analogous oxidation

of C–H bonds under Kharasch-Sosnovsky conditions,[38,39] involves inner-sphere coupling of the alkyl radical with the Cu complex, forming a formal Cu(III)-alkyl complex. Subsequent reductive elimination would then produce the *N*-alkylamide and a Cu(I) monoamidate. A third possible mechanism involves outer-sphere attack by the alkyl radical directly at the nitrogen atom of a bound amidate ligand, forming the *N*-alkyl amide and reforming the Cu(I) monoamidate in a single step. An analogous outer-sphere mechanism was suggested for an enantioconvergent C(sp^3)–N bond-forming reaction with a sterically-congested Cu-catalyst.[40] To discriminate between these competing pathways, each mechanism was computed for a set of four alkyl radicals with varying steric and electronic properties (methyl, ethyl, isopropyl and *tert*-butyl).

SET pathway. We first evaluated a potential SET pathway. However, this pathway was quickly ruled out based on the highly endergonic electron transfer between 54.8–114.2 kcal mol^{-1} (see SI Table S5). We attribute this high energy to the high ionization potentials of these non-stabilized alkyl radicals.[41] The particle-hole interaction in the complex formed between the reduced Cu(phen)$(NHBz)_2$ species and the oxidized alkyl radical (ca. –26 kcal mol^{-1} for $^tBu^+$) is insufficient to overcome the thermodynamic cost of electron transfer, leading to the conclusion that the reaction does not occur by an SET mechanism.

Inner-sphere pathway. Inner-sphere coupling of each of the four alkyl radicals to the d^9 Cu(II) bisamidate complex is predicted to be endergonic, spanning +3.2 to +12.7 kcal mol^{-1} from $Me^•$ to $^tBu^•$. This association generates a formally Cu(III)-alkyl complex in which the amidate ligands are disposed in a *cis* configuration (Figure 4a), and is electronically barrierless according to a potential energy scan with methyl radical (see SI Figure S6). Each complex adopts a distorted square pyramidal geometry at Cu, characterized by τ_5 values ranging from 0.17–0.29 across the series of alkyl radicals studied here (see SI Table S6–S7), in which τ_5=0 corresponds to a square pyramidal (C_{4v}) geometry and τ_5=1 corresponds to a trigonal bipyramidal (D_{3h}) geometry.[42] The axial position is occupied by one N atom of the phen ligand, and the long Cu–N_{ax} distance suggests that this interaction is weak and exists due to the geometric constraint enforced by the rigidity of the bidentate phen ligand. In a formally d^8 Cu(III) C_{4v} complex, the Cu $d_{x^2-y^2}$ orbital is vacant, and this vacancy should favor the square pyramidal geometry. However, analysis of the oxidation state of the copper with the OSLO method[43] suggests an ambiguous assignment of +2 or +3, indicating partial $d_{x^2-y^2}$ occupancy through Cu–C covalency. Distortion of the complex towards a trigonal bipyramidal geometry lowers the energy of the $d_{x^2-y^2}$ orbital, strengthening the Cu–C bond and lowering the total energy of the structure in the process (*vide infra*). Ligand steric effects may also contribute to the distortion away from a perfect C_{4v} geometry.

Reductive elimination from the *cis* Cu(III)-alkyl complexes occurs with barriers ranging from 9.7–13.6 kcal mol^{-1} (Figure 4b) and is strongly exergonic, with driving forces relative to the preceding Cu(III)-alkyl intermediate spanning –55.1 to –58.6 kcal mol^{-1}. However, in all cases, this reductive elimination is outcompeted by a polytopal rearrangement that leads to the corresponding *trans* Cu bisamidate complex (Figure 4c). This rearrangement is highly asynchronous (Figure 4c, inlay), characterized by initial motion of the alkyl ligand into the vacant axial site of the square pyramidal complex, followed by movement of one amide ligand into the equatorial site vacated by the alkyl ligand. An alternative rearrangement during which an *N*-bound amidate changes into an *O*-bound imidate is disfavored by at least 8 kcal mol^{-1} (see SI Table S8).

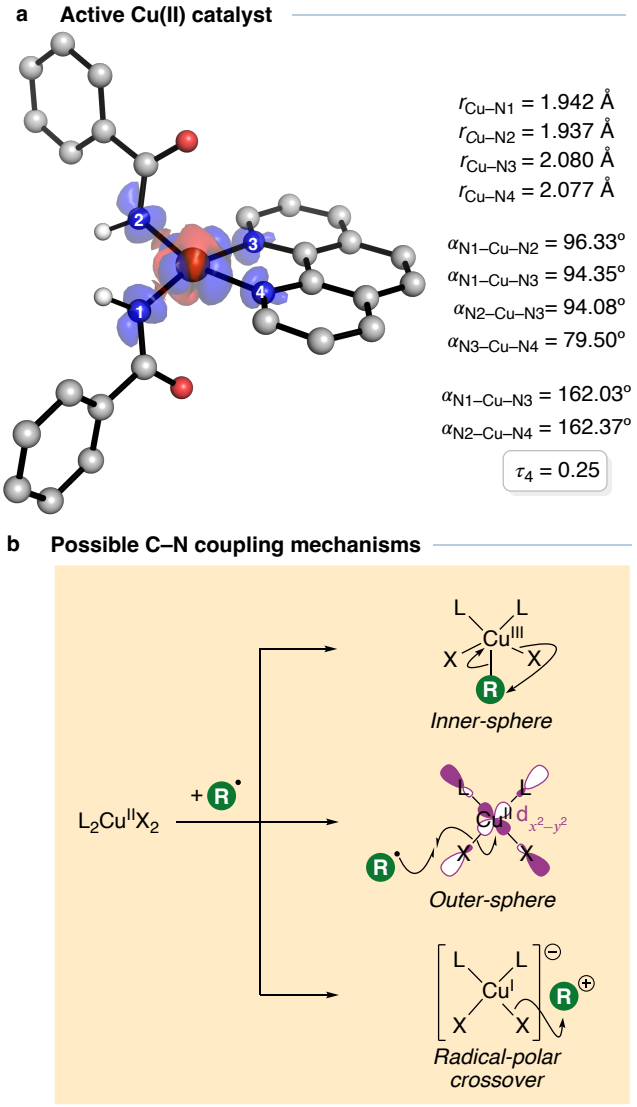

Figure 3. a. Structure and spin density of the active (phen)Cu(NHBz)$_2$ catalyst, calculated at the CPCM(C_6H_6)-wB97M-V/def2-TZVPP//CPCM(C_6H_6)-wB97M-V/B1 level (see SI for details).[44–46] Spin density plotted at an isovalue of 0.05 a.u. Hydrogen atoms hidden for clarity. **b.** Competing mechanisms for Cu-catalyzed C–N bond formation.

The polytopal isomerization process is exergonic for the reaction of each alkyl radical, with driving forces ranging from –1.2 to –5.0 kcal mol^{-1} (Figure 4d). We suggest that the *trans* isomer is favored over the *cis* isomer due to the stabilization from placing the most s-donating ligand (the alkyl ligand) *trans* to the least s-donating ligand (the phen ligand). This *trans* influence is manifested by a lengthening of the Cu–N_{eq} bond to the phen ligand by 0.02–0.06 Å in the *trans* complexes over that in the analogous *cis* isomers and shortening of the amidate Cu–N bond in the *trans* complex by 0.05–0.09 Å (see SI Table S6–S7) for complexes formed from each of the alkyl radicals. The large span of τ_5 values for the *trans* isomer (0.03–0.33) compared with those of the *cis* complexes (0.17–0.29) reflects the greater flexibility of the *trans* structure to accommodate alkyl ligands with varying steric requirements.

Reductive elimination from the *trans* Cu-alkyl complex of each alkyl ligand occurs with a lower barrier than from the *cis* complex (Figure 4e, 9.1–11.7 kcal mol^{-1}), despite the shorter, stronger Cu–C bond in each case

(*vide infra*). The sole exception to this trend is the complex of the methyl, the least sterically demanding of the alkyl groups.

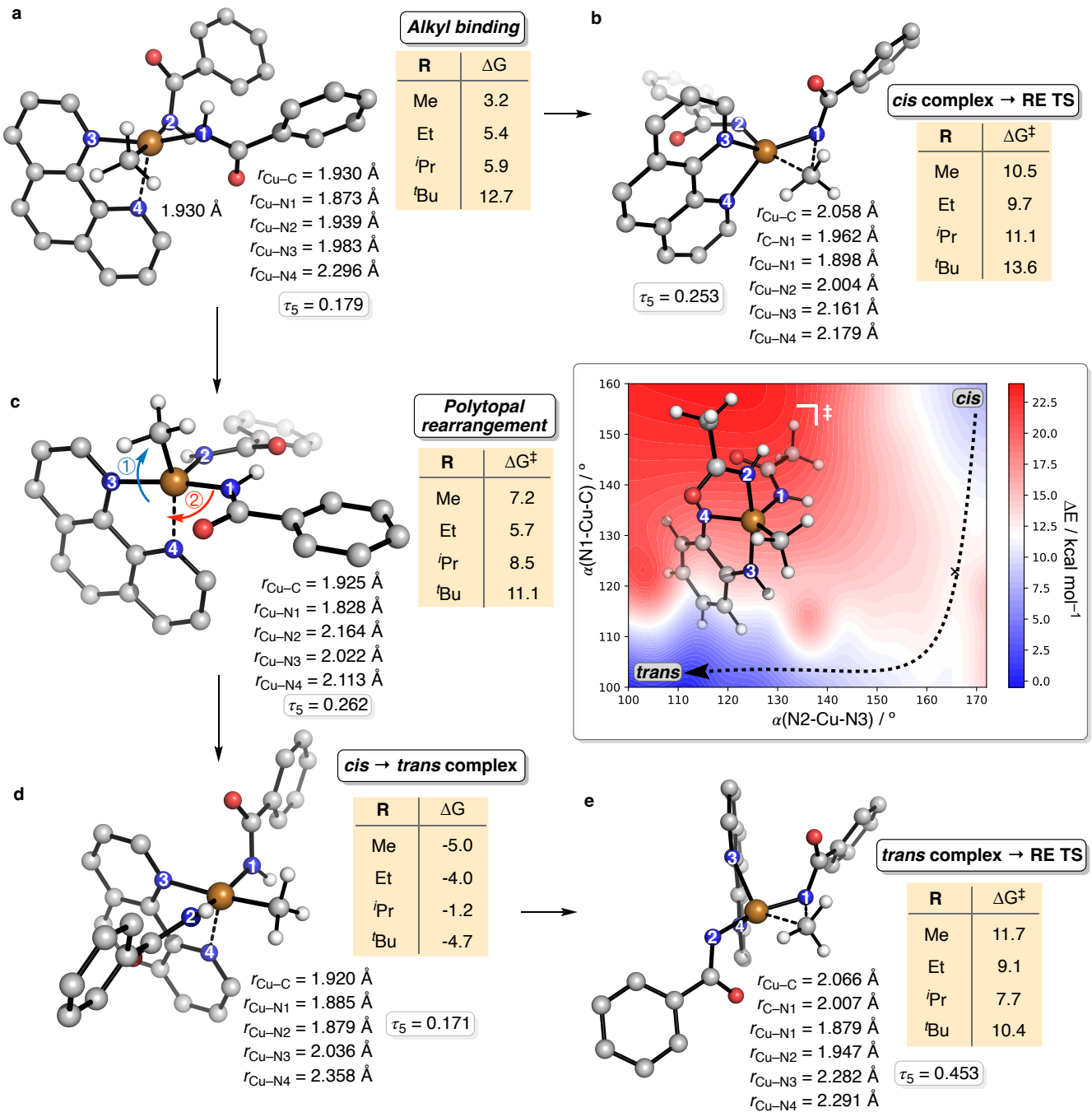

Figure 4. a. Free energy changes (kcal mol^{-1}) for alkyl radical binding to (phen)Cu(NHBz)$_2$ to form *cis*-(phen) Cu(NHBz)$_2$(Me). **b.** Reductive elimination free energy barriers (kcal mol^{-1}) relative to the preceding *cis*-(phen)Cu(NHBz)$_2$(Me) intermediate. **c.** Polytopal rearrangement transition state to interconvert between *cis*- and *trans*-(phen)Cu(NHBz)$_2$(Me). Inlay: Model potential energy surface illustrating the asynchronous nature of the polytopal rearrangement. **d.** Free energy change (kcal mol^{-1}) for the interconversion from *cis*- to *trans*-(phen)Cu(NHBz)$_2$(Me). **e.** Reductive elimination free energy barriers (kcal mol^{-1}) relative to the preceding *trans*-(phen)Cu(NHBz)$_2$(Me) intermediate. Free energies calculated at the CPCM(C_6H_6)-wB97M-V/def2-TZVPP//CPCM(C_6H_6)-wB97M-V/B1 level (393.15 K, 1 M). Hydrogen atoms hidden for clarity.

Analysis of the relationship between the nature of the Cu–C bond, the steric bulk of the alkyl substituent, and the barrier to reductive elimination was conducted with the absolutely localized molecular orbital energy decomposition analysis scheme (ALMO-EDA) for bonded interactions (Figure 5).[47,48] With this method, the interaction between geometrically-distorted and rehybridized open-shell fragments—in this case the alkyl radical and the Cu(II) bisamidate complex—are decomposed into their constituent parts: the 'frozen' interaction (ΔE_{FRZ}), which comprises Pauli repulsions, permanent electrostatics, and dispersion interactions; the spin-coupling of these fragments (ΔE_{SC}), which describes the covalency of the Cu–C bond; orbital polarization (ΔE_{POL}), which captures contraction and induced electrostatic interactions; and charge-transfer effects (ΔE_{CT}), which describe the ionic character of the bond (see SI for further discussion).

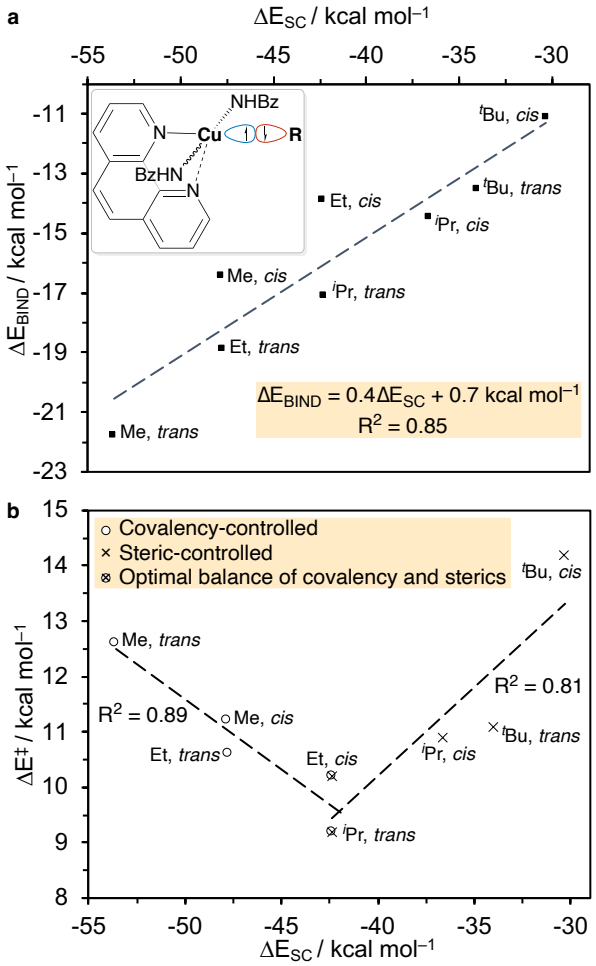

Figure 5. Relationship between Cu–C covalency (ΔE_{SC}), and Cu/alkyl binding (ΔE_{BIND}, **a**) and the reductive elimination barrier ($\Delta E^{‡}$, **b**), calculated at the wB97M-V/def2-TZVPP using the ALMO-EDA scheme for bonded interactions.

The primary source of variance in the total energy for binding of the alkyl group in the *cis*- and *trans*-(phen)Cu(NHBz)$_2$(R) complexes, ΔE_{BIND}, is described by the strength of the covalent Cu–C interaction (ΔE_{SC}, Figure 5a and SI Figure S8), in alignment with the result of the OSLO method that predicts a nonpolar covalent Cu–C bond (*vide supra*). We hypothesized that a stronger covalent Cu–C interaction will increase the activation barrier for reductive elimination because this bond breaks during the C–N bond-forming process.

A segmented linear regression plot of $\Delta E^{\ddagger}$ vs ΔE_{SC} (Figure 5b) reveals a negative correlation for complexes with strong spin coupling (ΔE_{SC} < –42.5 kcal mol^{-1}). However, for weaker spin coupling (ΔE_{SC} > –42.5 kcal mol^{-1}) the opposite is true: weaker spin coupling correlates with an *increase* in the activation barrier. This V-shaped relationship between ΔE_{SC} and the barrier to reductive elimination can be understood as follows: as alkyl radical substitution increases, Cu–C covalency, and, therefore, the strength of the Cu–C interaction, decreases. This bond weakening causes a lower barrier to reductive elimination. However, such an increase in substitution may also *inhibit* C–N bond formation due to increased steric repulsion with the amide ligand in the TS for reductive elimination. These effects of covalency and steric repulsion act antagonistically, resulting in the observed V-shaped relationship between ΔE_{SC} and $\Delta E^{\ddagger}$. Such a relationship is analogous to Sabatier's principle,[49] in this case with the lowest barrier resulting from the optimal balance of covalency and steric bulk in the Cu–alkyl complex. This optimal balance occurs with the secondary (isopropyl) radical in the *trans* Cu complex.

Outer-sphere pathway. We next characterized the pathway in which outer-sphere formation of the C–N bond occurs with each alkyl radical (Figure 6). Informed by the calculated spin density of the Cu(II) bisamidate (Figure 3a), TSs corresponding to attack of the alkyl radical on the Cu–N $\boldsymbol{\sigma}^*$ orbital were identified. Due to significant open-shell character of each TS, we employed Yamaguchi's approximate spin-projection scheme to estimate the activation barrier to C–N bond formation with the spin-pure singlet states (see SI for details).[50] Counter to the expectation based on the Bell-Evans-Polanyi principle,[51,52] the computed activation barrier for the outer-sphere coupling (17.7–21.0 kcal mol^{-1}) *decreased* as the driving force for C–N bond formation decreased. The driving force for C–N bond formation is lower for more substituted radicals, due to the greater stability from such substitution (Figure 6a).

We investigated the origin of this trend using the bonded ALMO-EDA method (*vide infra*) in combination with the distortion-interaction/activation-strain model.[53] We hypothesized that the polar character of the transition state will increase as the substitution of the radical increases, and this greater polar character should create an increase in the magnitude of $\Delta E^{\ddagger}_{CT}$. Since this term also depends on the position of the TS along the reaction coordinate, we normalized $\Delta E^{\ddagger}_{CT}$ using the frozen interaction ($\Delta E^{\ddagger}_{FRZ}$), which increases as the TS becomes more advanced, due to increased non-bonded repulsions. The variation in TS polarity can then be described by the ratio $\Delta E^{\ddagger}_{CT}/\Delta E^{\ddagger}_{FRZ}$, whose magnitude will increase as the TS becomes more polar. The positive relationship between $\Delta E^{\ddagger}$ and $\Delta E^{\ddagger}_{CT}/\Delta E^{\ddagger}_{FRZ}$ (Figure 6b) supports the interpretation that the barrier to C–N bond formation with a more substituted alkyl radical is lower because of the greater ability of the more substituted radical to stabilize positive charge. The increase in partial charge of the alkyl group at the TS supports this conclusion (see SI Figures S10–S11). The resulting increase in polarity causes an earlier, lower-energy TS, illustrated by the decrease in the forming bond length at the TS, $r^{\ddagger}_{C-N}$, as charge transfer decreases (Figure 6c). The increased steric bulk of more substituted radicals, therefore, is relatively unimportant at the TS of this mechanism, due to the longer bond that is forming.

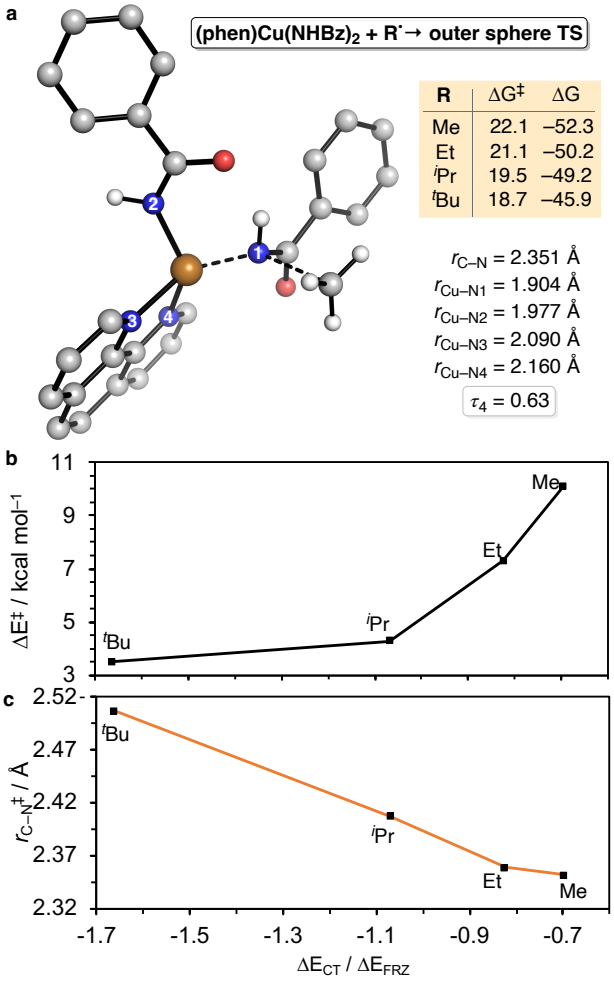

Figure 6. a. Outer-sphere alkyl radical addition process to (phen)Cu(NHBz)$_2$. Free energies calculated at the CPCM(C_6H_6)-wB97M-V/def2-TZVPP//CPCM(C_6H_6)-wB97M-V/B1 level (393.15 K, 1 M). Hydrogen atoms hidden for clarity. **b.** Contribution of TS polarity in the outer-sphere addition, characterized by the extent of charge transfer through the metric $\Delta E^{\ddagger}_{CT}/\Delta E^{\ddagger}_{FRZ}$. **c.** An earlier transition state results from an increase in transition state polarity. $\Delta E^{\ddagger}_{CT}$ and $\Delta E^{\ddagger}_{FRZ}$ calculated at the wB97M-V/def2-TZVPP level using the ALMO-EDA method for bonded interactions.

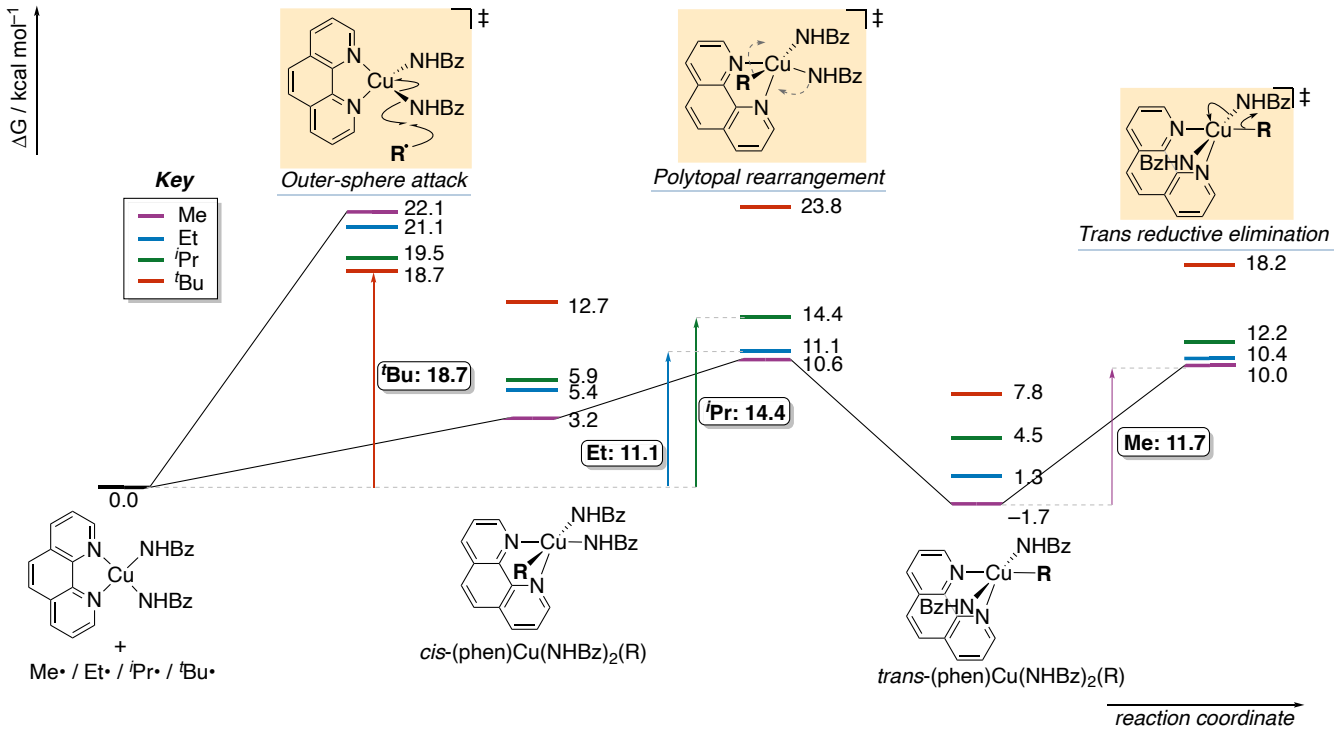

Figure 7. Simplified potential energy surface describing the fate of methyl, ethyl, isopropyl and *tert*-butyl radicals, calculated at the CPCM(C_6H_6)-wB97M-V/def2-TZVPP//CPCM(C_6H_6)-wB97M-V/B1 level (393.15 K, 1 M). Limiting activation barriers for each substrate are shown with vertical arrows. For full PES of each radical, see SI Figures S13–S16.

Operative C–N bond-forming pathways. Having characterized each of the potential reaction pathways, we directly compared the relative reactivity of methyl, ethyl, isopropyl and *tert*-butyl radicals to uncover the dominant mechanism in each case (Figure 7). According to our calculations, the overall trend in barrier for reaction of the alkyl radical with the copper amidate complex is ethyl (11.1) ≈ methyl (11.7) < isopropyl (14.4) < *tert*-butyl (18.7) [numbers in parentheses are the activation free energies (kcal mol^{-1}) relative to the lowest energy intermediate for each substrate]. For reactions with ethyl, isopropyl, and *tert*-butyl radicals, the lowest-energy intermediate along the reaction coordinate is the combination of the isolated (phen)Cu(NHBz)$_2$ complex and free alkyl radical, but for the methyl radical the minimum energy complex is *trans*-(phen)Cu(NHBz)$_2$(Me), reflective of the low stability of the methyl radical.

For methyl, ethyl, and isopropyl radicals, the inner-sphere mechanism is dominant, with relative activation free energies ($\Delta\Delta G^{‡}$) 5.1–10.4 kcal mol^{-1} lower than those of the alternative outer-sphere mechanism. The preference for the inner-sphere pathway decreases as the radical becomes more substituted, and reaction of the *tert*-butyl radical even favors outer sphere combination of the radical with the amidate ($\Delta\Delta G^{‡}$ = –5.1 kcal mol^{-1} favoring the outer-sphere pathway). According to our discussion earlier in this paper (Figure 4 and Figure 5), this change in mechanism results from the interplay of Cu–C covalency, steric bulk, and electrophilicity that accompanies an increase in radical substitution. For the most substituted radicals, the greater degree of substitution leads to steric bulk that inhibits the formation and rearrangement of the inner-sphere complex and stabilizes the outer-sphere TS by enhancing the effects of polarity during C–N bond formation. These effects combine to cause a large enough span in activation barriers to switch the reaction mechanism

from inner-sphere to outer-sphere.In summary, small, alkyl radicals undergo C–N bond formation by an inner-sphere mechanism involving reductive elimination from a copper intermediate containing an alkyl and amidate group, whereas the bulkiest substrates form the C–N bond by an outer sphere mechanism involving direct formation of the C–N bond without a copper-alkyl intermediate because the larger volume inhibits combination with the metal center.

Comparing the limiting activation barriers for each of these radicals to the computed HAT barriers (see SI Figure S12), we find that HAT is turnover limiting for methyl, ethyl and isopropyl radicals, in agreement with the results of previous kinetic isotope experiments with cyclohexane as substrate.[15] However, we predict that HAT from the 3° C–H bonds in isobutane should occur with a lower barrier than outer-sphere trapping of the resulting *tert*-butyl radical ($\Delta G^{\ddagger}$ = 16.7 vs 18.7 kcal mol^{-1}, respectively). Therefore, we predict that the turnover-limiting step for the bulkiest alkyl radicals will change from HAT to C–N bond formation. The inefficiency of C–N bond formation likely causes the low yields for reactions of bulky alkanes as radical decomposition becomes faster than formation of the C–N bond.

Effect of ligand electronics. To assess the validity of our computational results, we investigated the effect of the ligand on the rate of C–N bond formation and compared the predictions by computation with experimental results (Figure 8). Electron-withdrawing groups are predicted to increase the rate of reductive elimination by destabilizing the formally Cu(III) intermediate, as illustrated by the negative correlation between the predicted activation barrier to reductive elimination from *cis*-(phen)Cu(NHBz)$_2$(Me) and the Hammett parameter σ for the substituents at the 4 and 7 positions of the phen ligand (Figure 8a).[54] Conversely, the polytopal rearrangement is expected to be slower for the ligands that are more electron deficient. We rationalize this trend based on anticipated strengthening and shortening of the Cu–N bond of the migrating amidate ligand as the electron density on Cu decreases. Varying the electronic properties of the ligand for a given substrate will balance these two effects, and we anticipate a V-shaped relationship whereby the limiting step in the formation of the C–N bond switches from the polytopal rearrangement to the reductive elimination step in which the two amide ligands are disposed *cis* to one another. We predict that either strongly electron-donating or electron-withdrawing ligands will, therefore, enhance the rate of C–N bond formation.

To probe this mechanistic hypothesis, we devised a radical clock experiment with the branched alkane 2,4-dimethylpentane (Figure 8b, see SI for derivation).[55] Measurement of the ratio of yields of the branched 1° product (**1-N**) and the *iso*-butyl benzamide (**^{i}Bu-N**), formed from β-scission of the 1° branched alkyl radical and subsequent trapping, enables analysis of the relative rate of C–N bond formation versus the rate of β-scission (eq 1). The bidentate ligand 2,2'-bipyrine, symmetrically substituted at the 4 and 4’ positions, was selected for this experiment due to the availability of these ligands with varying electronic properties and their similarity to the phen ligand used for the computational studies above.

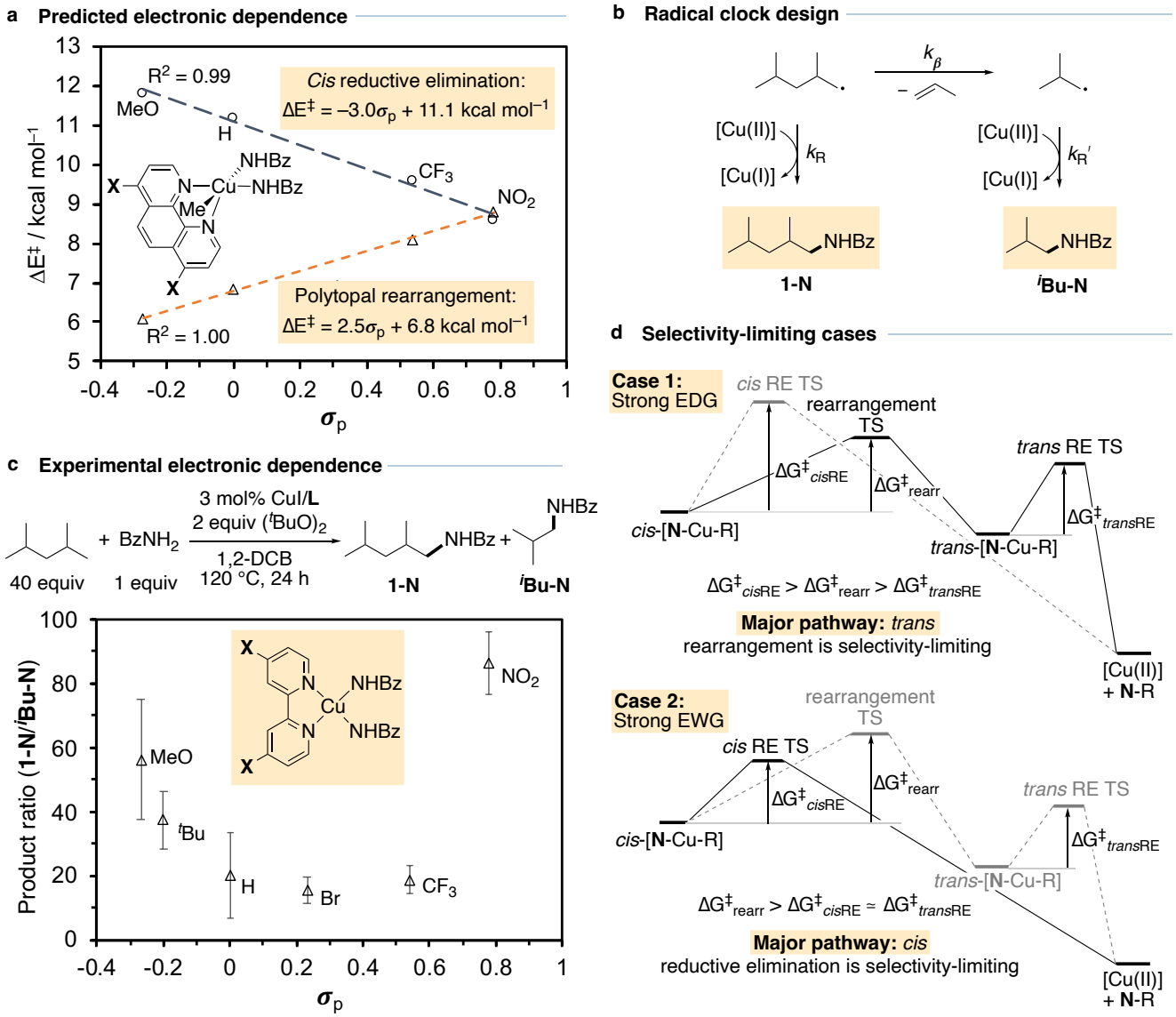

Figure 8. a. Computed relationship between ligand electronics and the rate of C–N bond formation, either through *cis* reductive elimination from (phen)Cu(NHBz)$_2$(Me) or via a polytopal rearrangement. **b.** Kinetic model to probe the rate of C–N bond formation using 2,4-dimethylpentane as a radical clock. **c.** Experimental results of the radical clock experiment indicating that both electron-rich and electron-deficient ligands increase the rate of C–N bond formation. Error bars represent ±1 standard deviation from the mean of the **1-N**/*i*-**Bu-N** ratio, which was run in triplicate. Conditions: 0.3 mmol benzamide, 9 μmol CuI, 9 μmol ligand, 12 mmol 2,4-dimethylpentane, 0.6 mmol (^{t}BuO)$_2$, 1,2-DCB, 120 °C, 20 h. Yields were determined by GC-FID. **d.** Schematic representation of the relationship between ligand electronics and the selectivity-determining step.

$$\frac{[\textbf{1-N}]}{[^i\textbf{Bu-N}]} = \frac{k_R[\text{Cu(II)}]}{k_\beta} \tag{1}$$

A plot of the ratio of [**1-N**]/[^{i}**Bu-N**] as a function of the Hammett parameter σ (Figure 8c) reveals a V-shaped relationship, in which either strongly electron-donating or electron-withdrawing substituents on the ligands lead to increased rates of C–N bond formation. While the yields for *iso*-butyl benzamide ^{i}**Bu-N** are low (<1%), this observed trend supports our prediction that the selectivity-determining step will change from the polytopal rearrangement with complexes of electron-donating ligands (*e.g.*, X=OMe) to the reductive elimination with

complexes of electron-deficient ligands (*e.g.*, X=NO_2). Ligands that are neither strongly electron-withdrawing nor electron-donating, for instance X=H or Br, cause the rate of C–N bond formation to be the lowest. The ligand with X=CN was a notable outlier in this series ([**1-N**]/[^{i}**Bu-N**]= 6.1 ± 3.6) and was omitted from the plot. Overall, these results point to two design principles for the development of novel organometallic catalysts for C–H amidation processes: first, ligand electronic properties can be used to modulate the rate of radical trapping to minimize β-scission byproducts, and, second, the catalyst coordination environment can be modified to avoid a high barrier to a required polytopal rearrangement (Figure 8d)

Conclusions

Methods for the selective, undirected functionalization of unactivated C–H bonds are highly desirable, but general principles for their development remain elusive. In this work, we have established a framework to uncover such principles using a combination of experimental and computational mechanistic studies, and energy decomposition analysis. Our conclusions from this approach are as follows:

1. The formation of the C–N bond with 1° and unhindered 2° radicals occurs by an inner-sphere mechanism. In this case, the yield and selectivity of the reaction is limited by the ability of the Cu complex to react with the alkyl radical to form a Cu–C bond, isomerize through a polytopal rearrangement, and undergo a subsequent reductive elimination.

2. For this inner-sphere mechanism, the polytopal rearrangement, as opposed to the subsequent reductive elimination, may be the selectivity-determining step in the C–N bond formation process.

3. The rate of the reductive elimination is highest for alkyl radicals that balance Cu–C covalency and steric bulk. Increasing radical substitution weakens the breaking Cu–C bond but increases the induced steric clash between the migrating alkyl group and the amide in the transition state.

4. For bulky alkyl radicals, for instance 3° radicals, the mechanism of C–N bond formation switches from inner-sphere to outer-sphere, due to a combination of increased steric congestion encountered in the inner-sphere mechanism, and stabilization of the outer-sphere transition state through polar effects.

5. The selectivity-determining step for C–N bond formation varies with the electronic properties of the ligand. The selectivity was shown to be determined by the barrier to rearrangement (Figure 8d, Case 1) with strongly electron-donating substituents on the ligand and to be determined by the barrier to reductive elimination with strongly electron-withdrawing substituents on the ligand (Figure 8d, Case 2). This change in ligand electronic properties causes a change in major pathway for the reaction.

Through this combined computational and experimental analysis, these principles can be used to guide the design of future C–H functionalization reactions that selectively install functional handles for late-stage functionalization efforts.

ASSOCIATED CONTENT

Supporting Information

The Supporting Information is available free of charge on the ACS Publications website.

Computational methods, experimental methods, supplementary figures and tables, NMR data (PDF)

Cartesian coordinates and energies of computed structures (zip)

AUTHOR INFORMATION

Corresponding Authors

* Alistair J. Sterling (ajsterling@lbl.gov); John F. Hartwig (jhartwig@berkeley.edu); Martin Head-Gordon (mhg@cchem.berkeley.edu)

Author Contributions

The manuscript was written through contributions of all authors. ‡These authors contributed equally.

Funding Sources

We acknowledge the UC Berkeley NMR facility and the National Institutes of Health for providing funding for the cryoprobe for the AV-600 spectrometer under grant S10OD024998. This work was supported by the U.S. Department of Energy, Office of Science, Office of Advanced Scientific Computing, and Office of Basic Science, via the Scientific Discovery through Advanced Computing (SciDAC) program, with additional support from the U.S. National Science Foundation through Grant No. CHE-1955643 and CHE-2313791. Experimental work was funded by the US Department of Energy, Office of Science, Office of Basic Energy Sciences, Materials Sciences and Engineering Division, under contract no. DE-AC02-05-CH11231, Unlocking Chemical Circularity in Recycling by Controlling Polymer Reactivity Across Scales program CUP-LBL-Helms.

ACKNOWLEDGMENT

We thank Dr. Abdulrahman Aldossary for discussions regarding OSLO calculations.

REFERENCES

(1) Dalton, T.; Faber, T.; Glorius, F. C-H activation: Toward sustainability and applications. *ACS Cent. Sci.* **2021**, *7*, 245–261.

(2) Yamaguchi, J.; Yamaguchi, A. D.; Itami, K. C-H bond functionalization: Emerging synthetic tools for natural products and pharmaceuticals. *Angew. Chem. Int. Ed.* **2012**, *51*, 8960–9009.

(3) Costas, M. Site and Enantioselective Aliphatic C−H Oxidation with Bioinspired Chiral Complexes. *Chem. Rec.* **2021**, *21*, 4000–4014.

(4) Davies, H. M. L.; Liao, K. Dirhodium tetracarboxylates as catalysts for selective intermolecular C–H functionalization. *Nat. Rev. Chem.* **2019**, *3*, 347–360.

(5) Karimov, R. R.; Hartwig, J. F. Transition-Metal-Catalyzed Selective Functionalization of C(sp3)−H Bonds in Natural Products. *Angew. Chem. Int. Ed.* **2018**, *57* (16), 4234–4241.

(6) Hong, B.; Luo, T.; Lei, X. Late-Stage Diversification of Natural Products. *ACS Cent. Sci.* **2020**, *6* (5), 622–635.

(7) Park, Y.; Kim, Y.; Chang, S. Transition Metal-Catalyzed C-H Amination: Scope, Mechanism, and Applications. *Chem. Rev.* **2017**, *117*, 9247–9301.

(8) Ramirez, T. A.; Zhao, B.; Shi, Y. Recent advances in transition metal-catalyzed sp3 C–H amination adjacent to double bonds and carbonyl groups. *Chem. Soc. Rev.* **2012**, *41*, 931–942.

(9) Collet, F.; Lescot, C.; Dauban, P. Catalytic C–H amination: The stereoselectivity issue. *Chem. Soc. Rev.* **2011**, *40*, 1926–1936.

(10) Fiori, K. W.; Du Bois, J. Catalytic intermolecular amination of C-H bonds: Method development and mechanistic insights. *J. Am. Chem. Soc.* **2007**, *129*, 562–568.
(11) Roizen, J. L.; Zalatan, D. N.; Du Bois, J. Selective intermolecular amination of C-H bonds at tertiary carbon centers. *Angew. Chem. Int. Ed.* **2013**, *52*, 11343–11346.
(12) Boquet, V.; Guimaraes Naves, J. A.; Brunard, E.; Nasrallah, A.; Joigneaux, M.; Sosa Carrizo, E. D.; Saget, T.; Darses, B.; Sircoglou, M.; Dauban, P. Rhodium(II)-Catalyzed Selective C(sp3)−H Amination of Alkanes. *Eur. J. Org. Chem.* **2023**, *26*, e202300352.
(13) Brunard, E.; Boquet, V.; Van Elslande, E.; Saget, T.; Dauban, P. Catalytic Intermolecular C(sp3)-H Amination: Selective Functionalization of Tertiary C-H Bonds vs Activated Benzylic C-H Bonds. *J. Am. Chem. Soc.* **2021**, *143*, 6407–6412.
(14) Lee, J.; Jin, S.; Kim, D.; Hong, S. H.; Chang, S. Cobalt-Catalyzed Intermolecular C-H Amidation of Unactivated Alkanes. *J. Am. Chem. Soc.* **2021**, *143*, 5191–5200.
(15) Tran, B. L.; Li, B.; Driess, M.; Hartwig, J. F. Copper-Catalyzed Intermolecular Amidation and Imidation of Unactivated Alkanes. *J. Am. Chem. Soc.* **2014**, *136*, 2555–2563.
(16) Fuentes, M. Á.; Gava, R.; Saper, N. I.; Romero, E. A.; Caballero, A.; Hartwig, J. F.; Pérez, P. J. Copper-Catalyzed Dehydrogenative Amidation of Light Alkanes. *Angew. Chem. Int. Ed.* **2021**, *60*, 18467–18471.
(17) Lusseau, J.; Robert, F.; Landais, Y. O-Methyl-N-nitroisourea as a NCO Surrogate in Cu-Catalyzed Alkane C–H Amidination. A Masked Isocyanate Strategy. *ACS Catal.* **2023**, *13*, 14257–14267.
(18) Pelletier, G.; Powell, D. A. Copper-catalyzed amidation of allylic and benzylic C-H bonds. *Org. Lett.* **2006**, *8*, 6031–6034.
(19) Wiese, S.; Badiei, Y. M.; Gephart, R. T.; Mossin, S.; Varonka, M. S.; Melzer, M. M.; Meyer, K.; Cundari, T. R.; Warren, T. H. Catalytic C - H amination with unactivated amines through copper(II) amides. *Angew. Chem. Int. Ed.* **2010**, *49*, 8850–8855.
(20) Teng, F.; Sun, S.; Jiang, Y.; Yu, J. T.; Cheng, J. Copper-catalyzed oxidative C(sp3)-H/N-H coupling of sulfoximines and amides with simple alkanes via a radical process. *Chem. Commun.* **2015**, *51*, 5902–5905.
(21) Wang, C. S.; Wu, X. F.; Dixneuf, P. H.; Soulé, J. F. Copper-Catalyzed Oxidative Dehydrogenative C(sp3)−H Bond Amination of (Cyclo)Alkanes using NH-Heterocycles as Amine Sources. *ChemSusChem* **2017**, *10*, 3075–3082.
(22) Zheng, Y. W.; Narobe, R.; Donabauer, K.; Yakubov, S.; König, B. Copper(II)-Photocatalyzed N-H Alkylation with Alkanes. *ACS Catal.* **2020**, *10*, 8582–8589.
(23) Chen, X.; Lian, Z.; Kramer, S. Enantioselective Intermolecular Radical Amidation and Amination of Benzylic C−H Bonds via Dual Copper and Photocatalysis. *Angew. Chem. Int. Ed.* **2023**, *62*, e202217638.
(24) Dai, L.; Chen, Y. Y.; Xiao, L. J.; Zhou, Q. L. Intermolecular Enantioselective Benzylic C(sp3)−H Amination by Cationic Copper Catalysis. *Angew. Chem. Int. Ed.* **2023**, *62*, e202304427.
(25) Ciccia, N. R.; Shi, J. X.; Pal, S.; Hua, M.; Malollari, K. G.; Lizandara-Pueyo, C.; Risto, E.; Ernst, M.; Helms, B. A.; Messersmith, P. B.; Hartwig, J. F. Diverse functional polyethylenes by catalytic amination. *Science* **2023**, *381*, 1433–1440.
(26) Kharasch, M. S.; Sosnovsky, G. The Reactions of t-Butyl Perbenzoate and Olefins—A Stereospecific Reaction. *J. Am. Chem. Soc.* **1958**, *80*, 756–756.
(27) Walling, C.; Jacknow, B. B. Positive Halogen Compounds. I. The Radical Chain Halogenation of Hydrocarbons by t-Butyl Hypochlorite 1. *J. Am. Chem. Soc.* **1960**, *82*, 6108–6112.
(28) Xia, Q.; Liu, X.; Zhang, Y.; Chen, C.; Chen, W. Copper-catalyzed N-methylation of amides and O-methylation of carboxylic acids by using peroxides as the methylating reagents. *Org. Lett.* **2013**, *15*, 3326–3329.
(29) Aynetdinova, D.; Callens, M. C.; Hicks, H. B.; Poh, C. Y. X.; Shennan, B. D. A.; Boyd, A. M.; Lim, Z. H.; Leitch, J. A.; Dixon, D. J. Installing the “magic methyl”-C-H methylation in synthesis. *Chem. Soc. Rev.* **2021**, *50*, 5517–5563.
(30) Agrawal, I.; Prakash, G.; Al-Thabaiti, S. A.; Mokhtar, M.; Maiti, D. C−H Methylation Using Sustainable Approaches. *Catalysts* **2022**, *12*, 510.
(31) Yang, L.; Powell, D. R.; Houser, R. P. Structural variation in copper(i) complexes with pyridylmethylamide ligands: Structural analysis with a new four-coordinate geometry index, τ4. *J. Chem. Soc. Dalt. Trans.* **2007**, *9*, 955–964.

(32) Raithby, P. R.; Shields, G. P.; Allen, F. H.; Motherwell, W. D. S. Structure correlation study of four-coordinate copper(I) and (II) complexes. *Acta Crystallogr. Sect. B Struct. Sci.* **2000**, *56*, 444–454.
(33) Sigel, H.; Huber, P. R.; Griesser, R.; Prijs, B. Ternary complexes in solution. XV. Mixed-ligand copper(II) complexes with 2,2'-bipyridyl or 1,10-phenanthroline and pyrocatecholate or derivatives thereof. *Inorg. Chem.* **1973**, *12*, 1198–1200.
(34) Sigel, H. Ternary Cu 2+ Complexes: Stability, Structure, and Reactivity. *Angew. Chem. Int. Ed.* **1975**, *14*, 394–402.
(35) Leyssens, T.; Peeters, D.; Orpen, A. G.; Harvey, J. N. How Important Is Metal - Ligand Back-Bonding toward YX 3. *Organometallics* **2007**, *26*, 2637–2645.
(36) Kochi, J. K. Electron-Transfer Mechanisms for Organometallic Intermediates in Catalytic Reactions. *Acc. Chem. Res.* **1974**, *7*, 351–360.
(37) Suh, S. E.; Chen, S. J.; Mandal, M.; Guzei, I. A.; Cramer, C. J.; Stahl, S. S. Site-Selective Copper-Catalyzed Azidation of Benzylic C-H Bonds. *J. Am. Chem. Soc.* **2020**, *142*, 11388–11393.
(38) Beckwith, A. L. J.; Zavitsas, A. A. Allylic Oxidations by Peroxy Esters Catalyzed by Copper Salts. The Potential for Stereoselective Syntheses. *J. Am. Chem. Soc* **1986**, *108*, 8230–8234.
(39) Andrus, M. B.; Lashley, J. C. Copper catalyzed allylic oxidation with peresters. *Tetrahedron* **2002**, *58*, 845–866.
(40) Zhang, Y.; Wang, J.; Yang, N.; Chen, Z.; Wang, L.; Gu, Q.; Li, Z.; Liu, X. Copper-Catalyzed Enantioconvergent Radical C(sp 3)−N Cross-Coupling: Access to α,α-Disubstituted Amino Acids. *Angew. Chem. Int. Ed.* **2023**, *62*, e202302983.
(41) Lias, S. G. Gas phase ion energetics data. In *NIST Chemistry WebBook, NIST Standard Reference Database Number 69*; P.J. Linstrom, Mallard, W. G., Eds.; National Institute of Standards and Technology: Gaithersburg MD. DOI: https://doi.org/10.18434/T4D303. Accessed 2023-09-05.
(42) Addison, A. W.; Rao, T. N.; Reedijk, J.; van Rijn, J.; Verschoor, G. C. Synthesis, structure, and spectroscopic properties of copper(II) compounds containing nitrogen–sulphur donor ligands; the crystal and molecular structure of aqua[1,7-bis(N-methylbenzimidazol-2′-yl)-2,6-dithiaheptane]copper(II) perchlorate. *J. Chem. Soc., Dalt. Trans.* **1984**, *7* (7), 1349–1356.
(43) Gimferrer, M.; Aldossary, A.; Salvador, P.; Head-Gordon, M. Oxidation State Localized Orbitals: A Method for Assigning Oxidation States Using Optimally Fragment-Localized Orbitals and a Fragment Orbital Localization Index. *J. Chem. Theory Comput.* **2022**, *18*, 309–322.
(44) Barone, V.; Cossi, M. Quantum Calculation of Molecular Energies and Energy Gradients in Solution by a Conductor Solvent Model. *J. Phys. Chem. A* **1998**, *102*, 1995–2001.
(45) Mardirossian, N.; Head-Gordon, M. ωB97M-V: A combinatorially optimized, range-separated hybrid, meta-GGA density functional with VV10 nonlocal correlation. *J. Chem. Phys.* **2016**, *144*, 214110.
(46) Weigend, F.; Ahlrichs, R. Balanced Basis Sets of Split Valence, Triple Zeta Valence and Quadruple Zeta Valence Quality for H to Rn: Design and Assessment of Accuracy. *Phys. Chem. Chem. Phys.* **2005**, *7*, 3297–3305.
(47) Levine, D. S.; Horn, P. R.; Mao, Y.; Head-Gordon, M. Variational Energy Decomposition Analysis of Chemical Bonding. 1. Spin-Pure Analysis of Single Bonds. *J. Chem. Theory Comput.* **2016**, *12*, 4812–4820.
(48) Levine, D. S.; Head-Gordon, M. Energy decomposition analysis of single bonds within Kohn–Sham density functional theory. *Proc. Natl. Acad. Sci.* **2017**, *114*, 12649–12656.
(49) Sabatier, P. Hydrogénations et déshydrogénations par catalyse. *Berichte der Dtsch. Chem. Gesellschaft* **1911**, *44*, 1984–2001.
(50) Yamaguchi, K.; Takahara, Y.; Fueno, T.; Houk, K. N. Extended Hartree-Fock (EHF) theory of chemical reactions - III. Projected Møller-Plesset (PMP) perturbation wavefunctions for transition structures of organic reactions. *Theor. Chim. Acta* **1988**, *73*, 337–364.
(51) Bell, R. P. The theory of reactions involving proton transfers. *Proc. R. Soc. London. Ser. A - Math. Phys. Sci.* **1936**, *154*, 414–429.
(52) Evans, M. G.; Polanyi, M. Inertia and Driving Force Of Chemical Reactions. *Trans. Faraday Soc.* **1938**, *34*, 11–24.
(53) Bickelhaupt, F. M.; Houk, K. N. Analyzing Reaction Rates with the Distortion/Interaction-Activation Strain Model. *Angew. Chem. Int. Ed.* **2017**, *56*, 10070–10086.

(54) Hammett, L. P. The Effect of Structure upon the Reactions of Organic Compounds. Benzene Derivatives. *J. Am. Chem. Soc.* **1937**, *59*, 96–103.
(55) Griller, D.; Ingold, K. U. Free-Radical Clocks. *Acc. Chem. Res.* **1980**, *13*, 317–323.

Graphic entry for the Table of Contents (TOC)